INFORMATICA, 2015, Vol. 26, No. 4, 621–634

DOI: http://dx.doi.org/10.15388/Informatica.2015.67

Image Motion Restoration Using Fractional-Order Gradient Prior

Ying FU[1], Xi WU[1]*, Xiaohua LI[2], Kun HE[2], Yi ZHANG[2], Jiliu ZHOU[1]
[1]*College of Computer Science, Chengdu University of Information Technology Chengdu, 610225, China*
[2]*College of Computer Science, Sichuan University, Chengdu, 610064, China*
e-mail: fuying@cuit.edu.cn, wuxi@cuit.edu.cn

Received: October 2013; accepted: March 2015

Abstract. The choice of natural image prior decides the quality of restored image. Recently successful algorithms exploit heavy-tailed gradient distribution as image prior to restore latent image with piecewise smooth regions. However, these prior assumed also remove the mid-frequency component such as textural details regions while they preserve sharp edges. That because gradient profile in fractal-like texture do not have sparse characteristic.

To restore textural features of expected latent image, in this paper, we introduce fractional-order gradient as image prior which is more appropriate to describe characteristic of image textures. From details comparison of our experiments, the textual details are more clear and visual quality is improved.

Key words: image motion restoration, fractional order, total variation, textural detail.

1. Introduction

Image motion blur resulting from camera shake is spatial uniform, which can be modeled as the convolution of the latent image and point-spread-function (a.k.a blur kernel) representing the track of camera moving:

$$\mathbf{Y} = \mathbf{X} \otimes \mathbf{h} + \mathbf{n} \tag{1}$$

where $\mathbf{Y}$ is observed blurred image, $\mathbf{X}$ is the latent image, $\mathbf{h}$ is the motion blur kernel,and $\mathbf{n}$ is the Gaussian noise with σ^2 variation, $\otimes$ denotes the convolution operator. When blur kernel is unknown, the restoration of latent image from single observed image is called the image blind deconvolution (Haykin, 1994) (a.k.a image blind motion deblurring).

Usually,image blind deconvolution has two steps: (1) blur kernel estimation and (2) given estimated blur kernel and observed image, to restore latent image. For the importance of first step, many researchers believe the more accurately blur kernel is estimated, the more clearly image is restored. However, in fact, even with exact blur kernel, the restoration of latent image is still challenging problem,because blur attenuates

*Corresponding author.

information such as high-frequency and mid-frequency components about image. So traditional methods such as inverse filtering and wiener filtering (Sekko *et al.*, 1999) always enlarge noise in order to restore high-frequency component. To suppress noise, Bar *et al.* (2005) used l_1 norm with a Mumford–Shah regularizer to reject salt-and-pepper noise. Joshi *et al.* (2009) introduced a local two-color prior to suppress noise. However, these methods proposed in Bar *et al.* (2005), Joshi *et al.* (2009) increase the computation cost to solve the nonlinear optimization problem using iterative re-weighted least square. Numerous regularization approaches have been proposed, too (Rudin and Osher, 1994; Chan and Wong, 1998; Wang *et al.*, 2008; Xu and Jia, 2010). Rudin and Osher (1994) proposed a time marching scheme to solve the TV model. Chan and Wong (1998) introduced total variational blind deconvolution method for motion blur kernel and out-of-focus kernel. Wang *et al.* (2008) presented a fast total variation deconvolution algorithm to compute TV image deconvolution. Xu and Jia (2010) developed a fast $\mathbf{TV} - l_1$ deconvolution method based on half-quadratic splitting. Fergus *et al.* (2006) estimate blur kernel by introducing heavy-tailed gradient prior of natural image based on variational Bayesian, and restore latent image using Richardson–Lucy (RL) approach with serious ring artifact. Rao and Chen (2012) discussed that some researchers used the global motion compensation from coarsely sampled motion vector fields to camera shift problem in video enhancement.

Algorithms above reconstruct the latent images with piecewise smooth characteristic and preserve the image edges, but meanwhile the mid-frequency components such as textures are removed too. Recently, online learning algorithms for neural networks will be considered to apply in image motion restoration (Calvo-Rolle *et al.*, 2014).

In digital images, the gray values between neighboring pixels have high correlation. These highly self-similar fractal information of image fractal information is usually represented by complex textural features, and the works in Pu *et al.* (2008), Yi-Fei *et al.* (2007), Jun and Zhihui (2011), Bai and Feng (2007), Zhang *et al.* (2011, 2012), Chan *et al.* (2013) showed that fractional-order gradient is more suitable to deal with fractal-like textures. It has been proved in Pu *et al.* (2008) that the fractional-order derivative satisfies the lateral inhibition principle of biologic visual system better than the integer-order derivative. The fractional-order derivative operators have been used in texture enhancement (Yi-Fei *et al.*, 2007), image denoising (Jun and Zhihui, 2011; Bai and Feng, 2007) and image inpainting (Zhang *et al.*, 2011, 2012). Jun and Zhihui (2011) replaced the first-order derivative in the regularized term of ROF model with the fractional-order derivative. Bai and Feng (2007) designed fractional-order anisotropic diffusion equation to remove noise. Zhang *et al.* (2011) exploited fractional-order TV sinogram inpainting model to reduce metal artifacts for **X**-ray computed tomography. In Chan *et al.* (2013) fractional total variation method was introduced to restore textured image, but fractional-order gradient prior is not always fit for Laplacian distribution. These works showed that the fractional-order derivative not only nonlinearly preserve the textural details in smooth area, but eliminate the staircase effect caused by low integral-order derivative in image processing.

In this paper, we use the blur kernel estimated by algorithm in Krishnan *et al.* (2011), and then propose a non-blind motion deblurring algorithm to reconstruct textural details

in latent image by exploiting the fractional-order gradient distribution of natural image as an image prior. The outline of this paper is as follows. In Section 2, analyze the reason why natural image gradient priors fails to restore image texture. In Section 3, our image deconvolution model is proposed and fractional-order gradient operator is constructed according to the *Grnüwald–Letnikov* definition of fractional-order derivative. In Section 4, based on half-quadratic splitting, we develop Bayesian MAP estimation image deconvolution method to compute variables iteratively. In Section 5, the restored results are shown and discussed. Finally, the conclusion of our work is in Section 6.

2. Motivation

Even with known kernel, recent approaches exploiting the sparse gradient prior or Gaussian gradient prior fails to reconstruct image with full textural details. The prior $p(\mathbf{X})$ favors natural image, usually based on the observation that their heavy-tailed gradient distribution is sparse. A common measure is

$$\log p(\mathbf{X}) = -\sum_i \left|\nabla_x(\mathbf{x}_i)\right|^\beta + \left|\nabla_y(\mathbf{x}_i)\right|^\beta + \text{const}, \tag{2}$$

where $\nabla_x(\mathbf{x}_i)$ and $\nabla_y(\mathbf{x}_i)$ denote the horizontal and vertical integral-order derivatives at pixel i. Exponent value $\beta < 1$ leads to sparse prior and natural images usually correspond to α in the range of $[0.5, 0.8]$ (Levin *et al.*, 2009). $\beta = 1$ and $\beta = 2$ are Laplacian prior and Gaussian prior, respectively.

During restoration process, unappropriate priors favor no-blurry explanation on image regions such as edge and textures. To understand the failure of restoring textural details with natural image gradient prior, consider the 1D signal s in Fig. 1.Sharp edge in Fig. 1(a) can be restored by gradient prior. Although Gaussian prior favors the blurry explanation, the sparse prior ($\alpha < 1$) favor the correct sharp explanation in Fig. 1(b). The signal considered in Fig. 1(c) is illustrating that natural image contain a lot of medium contrast textures, which dominates the statistics more than step edges. As a result, blurring natural image reduces the overall contrast which cannot be restored by Gaussian prior or even sparse priors can not restore as in Fig. 1(d)

The reason is that the gradient profile in fractal-like textures is close to Gaussian distribution and these small values are severely penalized by the sparse gradient prior.

A fractional-order gradient l*og* distribution can be expressed as follows

$$\log p(\mathbf{X}) = -\sum_i \left|\nabla_x^v \mathbf{x}_i\right|^\beta + \left|\nabla_y^v \mathbf{x}_i\right|^\beta + \text{const}, \tag{3}$$

where $\nabla_x^v \mathbf{x}_i$ and $\nabla_y^v \mathbf{x}_i$ denote the horizontal and vertical fractional-order derivatives at pixel i and v is the fractional order. The exponent value is the same as β value in Eq. (2).

In our analysis, $v = 0.3$ is chosen. Compared with result in Fig. 2(b), the sharp explanation in Fig. 2(c) is favored by sparse prior even by Gaussian prior. The fractional-order gradient prior with appropriate fractional order chosen can restore textural details successfully.

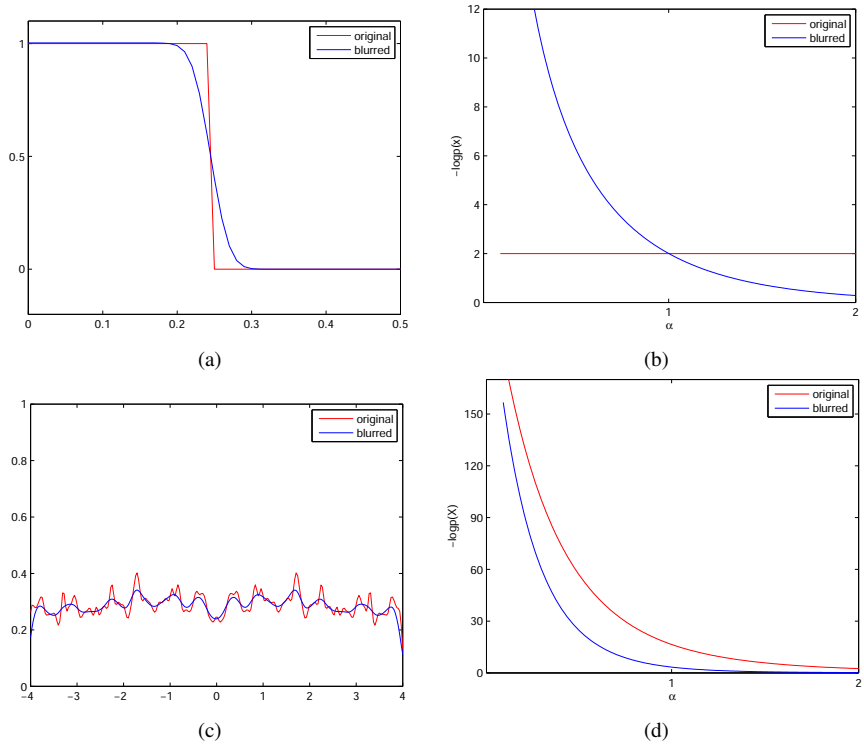

Fig. 1. Analysis of restoration on 1D signal using first-order gradient prior: (left): sharp and blurred signal; (right): sum of gradients $-\log p(\mathbf{X}) = \sum_i |\nabla(\mathbf{x})_i|^{\beta}$ as a function of β.

3. Image Deconvolution

Before our algorithm is proposed ,the blur kernel is estimated by algorithm in Krishnan *et al.* (2011), which introduces a minimization scheme $\frac{l_1}{l_2}$ that solve a series of l_1 problems with different regularization parameters and estimate $\mathbf{X}$ and $\mathbf{h}$ iteratively. The image reconstructed with this blur kernel estimated in Krishnan *et al.* (2011) without any ring artifacts. This serious undesirable phenomena will show in image reconstructed by algorithm in Fergus *et al.* (2006), which result from the uncorrect estimation on blur kernel. The importance of blur kernel estimation is showed in Fig. 3.

3.1. *Model of Image Non-Blind Restoration*

Motivated by works of Chan *et al.* (2013), Krishnan *et al.* (2011) and our analysis above, we introduce a fractional-order gradient as image prior. The Bayesian estimator combines both the prior and data knowledge, the model is defined as follows:

$$p(\mathbf{X}|\mathbf{Y},\mathbf{h}) \propto p(\mathbf{Y},\mathbf{h}|\mathbf{X})\,p(\mathbf{X}) \tag{4}$$

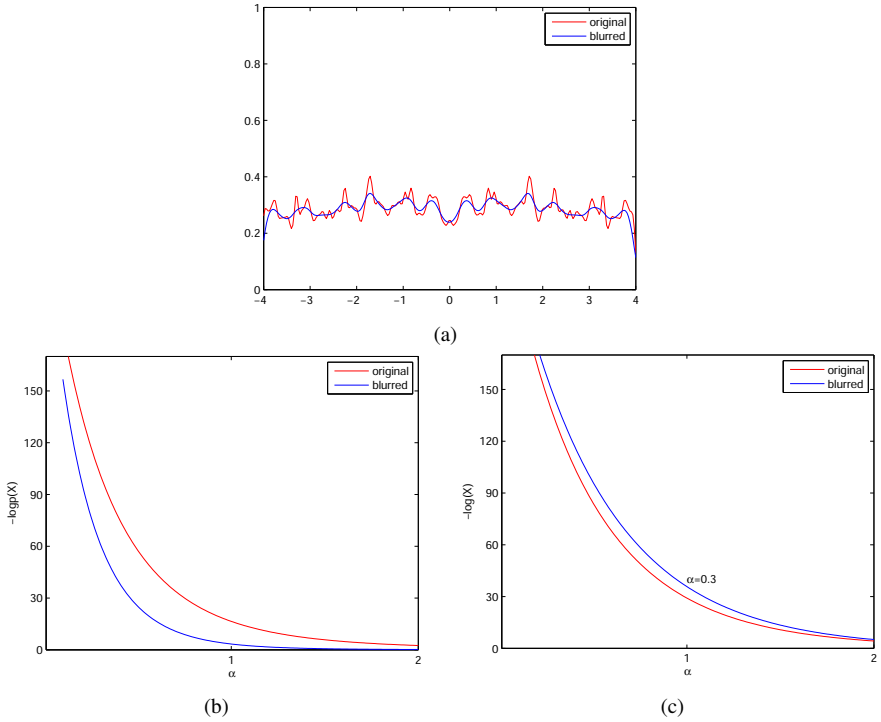

Fig. 2. Comparison of restoration on signal representing image texture: (a) sharp and blurred signal; (b) sum of gradients $-\log p(\mathbf{X}) = \sum_i |\nabla^v(\mathbf{x})_i|^\beta$ as a function of β; (c) sum of gradients $-\log p(\mathbf{X}) = \sum_i |\nabla^v(\mathbf{x})_i|^\beta$ as a function of β.

where $p(\mathbf{Y}, \mathbf{h}|\mathbf{X})$ being a Gaussian likelihood, their log distribution is $\log p(\mathbf{Y}, \mathbf{h}|\mathbf{X}) = -\|\mathbf{X} \otimes \mathbf{h} - \mathbf{Y}\|_2^2$ and $\log p(\mathbf{X}) = -\sum_i |\nabla_x^v \mathbf{x}_i|^\beta + |\nabla_y^v \mathbf{x}_i|^\beta$, ∇_x^v and ∇_y^v are the same derivative filters in Eq. (3).

In fact, Bayesian MAP approach in Eq. (4) amounts to the minimization of the posterior energy, so Eq. (4) can rewritten as

$$\begin{aligned}\hat{\mathbf{X}} &= \arg\min_{\mathbf{X}} \sum_i \left(\lambda \|\mathbf{x}_i \otimes \mathbf{h} - \mathbf{y}_i\|^2 + \left|\nabla_x^v \mathbf{x}_i\right|^\beta + \left|\nabla_y^v \mathbf{x}_i\right|^\beta\right) \\ &= \arg\min_{\mathbf{X}} \sum_i \left(\lambda \|\mathbf{x}_i \otimes \mathbf{h} - \mathbf{y}_i\|^2 + \left|\mathbf{x}_i \otimes D_x^v\right|^\beta + \left|\mathbf{x}_i \otimes D_y^v\right|^\beta\right),\end{aligned} \tag{5}$$

where $\nabla_x^v \mathbf{x} = \mathbf{x} \otimes D_x^v$, $\nabla_y^v \mathbf{x} = \mathbf{x} \otimes D_y^v$ and D^v is the fractional-order derivative filters constructed in following.

3.2. *Fractional-Order Derivative Filter Operator*

The fractional-order gradient operator is constructed by the discretion of the *Grnüwald–Letnikov* definition of fractional-order derivative. The v-order definition based fractional

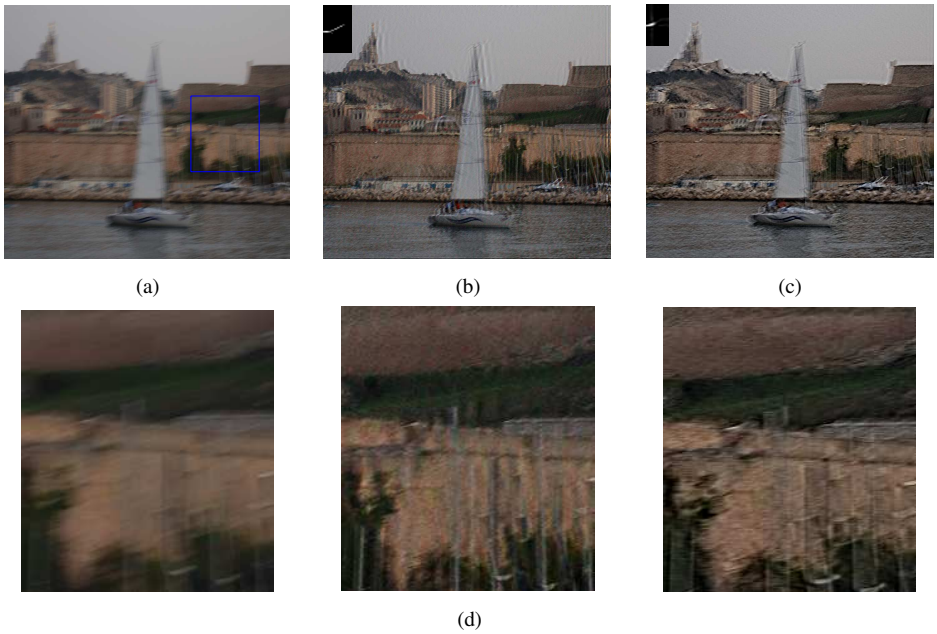

Fig. 3. The effect of estimated blur kernel on restored image: (a) blurred image; (b) latent image given blur kernel estimated in Fergus *et al.* (2006); (c) latent image given blur kernel estimated in Krishnan *et al.* (2011); (d) details comparison on image window, left: details in (a), middle: details in (b), right: details in (c).

differential can be expressed as

$$D_{GL}^{v} = \frac{d^{v}}{[d(x-a)]^{v}}\bigg|_{GL} = \lim_{N\to\infty}\sum_{k=0}^{N-1}\frac{\Gamma(k-v)}{\Gamma(k+1)}s\left(x-k\left(\frac{x-a}{N}\right)\right) \tag{6}$$

where $x \in [a, x]$, $x - k(\frac{x-a}{N})$ is the discrete sampling. For large N and $a = 0$, rewrite Eq. (6) as

$$\frac{d^{v}}{dx^{v}}\bigg|_{G-L} \cong \frac{x^{-v}N^{v}}{\Gamma(-v)}\sum_{k=0}^{N-1}\frac{\Gamma(k-v)}{\Gamma(k+1)}s\left(x-\frac{kx}{N}\right) = \frac{x^{-v}N^{v}}{\Gamma(-v)}\sum_{k=0}^{N-1}\frac{\Gamma(k-v)}{\Gamma(k+1)}s_{k}. \tag{7}$$

For faster execution speeds and better precision of convergence, Eq. (7) can be rewritten as

$$\frac{d^{v}}{dx^{v}}\bigg|_{G-L} \cong \frac{x^{-v}N^{v}}{\Gamma(-v)}\sum_{k=0}^{N-1}\frac{\Gamma(k-v)}{\Gamma(k+1)}s\left(x+\frac{vx}{2N}-\frac{kx}{N}\right) \tag{8}$$

To get these signal value of $s(x)$ on non-nodes, we use the Lagrange 3-point interpolation using three neighboring nodes $s(x - \frac{x}{N} - \frac{kx}{N})$, $s(x - \frac{kx}{N})$, $s(x + \frac{x}{N} - \frac{kx}{N})$. The value of

$x(\varepsilon)$ can be gotten as follows

$$\begin{aligned} s(\varepsilon) \cong\ & \frac{(\varepsilon - x + \frac{kx}{N})(\varepsilon - x + \frac{x}{N} + \frac{kx}{N})}{2x^2/N^2} s\left(x + \frac{x}{N} - \frac{kx}{N}\right) \\ & - \frac{(\varepsilon - x - \frac{x}{N} + \frac{kx}{N})(\varepsilon - x + \frac{x}{N} + \frac{kx}{N})}{2x^2/N^2} s\left(x - \frac{kx}{N}\right) \\ & + \frac{(\varepsilon - x - \frac{x}{N} + \frac{kx}{N})(\varepsilon - x + \frac{kx}{N})}{2x^2/N^2} s\left(x - \frac{x}{N} - \frac{kx}{N}\right). \end{aligned} \tag{9}$$

Assuming $\varepsilon = vx/N - kx/N$ and performing fractional interpolation

$$\begin{aligned} s\left(x + \frac{vx}{2N} - \frac{kx}{N}\right) &\cong \left(\frac{v}{4} + \frac{v^2}{8}\right) s\left(x + \frac{x}{N} - \frac{kx}{N}\right) + \left(1 - \frac{v^2}{4}\right) s\left(x - \frac{kx}{N}\right) \\ &\quad + \left(\frac{v^2}{8} - \frac{v}{4}\right) s\left(x - \frac{x}{N} - \frac{kx}{N}\right) \\ &= \left(\frac{v}{4} + \frac{v^2}{8}\right) s_{k-1} + \left(1 - \frac{v^2}{4}\right) s_k + \left(\frac{v^2}{8} - \frac{v}{4}\right) s_{k+1}. \end{aligned} \tag{10}$$

Setting $k = n \ll N - 1$, from Eq. (10) the anterior $n + 2$ approximate backward difference of the fractional partial differentials with respect to the negative x- and y-axes of two dimensional signals $s(x, y)$ can be expressed as

$$\begin{aligned} \frac{\partial^v s(x, y)}{\partial x^v} \cong\ & \left(\frac{v}{4} + \frac{v^2}{8}\right) s(x + 1, y) + \left(1 - \frac{v^2}{2} - \frac{v^3}{8}\right) s(x, y) + \frac{1}{\Gamma(-v)} \\ & \times \sum_{k=1}^{n-2} \left[\frac{\Gamma(k - v - 1)}{(k + 1)!} \cdot \left(\frac{v}{4} + \frac{v^2}{8}\right) + \frac{\Gamma(k - v)}{k!} \cdot \left(1 - \frac{v^2}{4}\right) \right. \\ & \left. + \frac{\Gamma(k - v - 1)}{(k - 1)!} \cdot \left(-\frac{v}{4} + \frac{v^2}{8}\right) \right] s(x - k, y) + \left[\frac{\Gamma(n - v - 1)}{(n + 1)!\Gamma(-v)} \right. \\ & \left. \times \left(1 - \frac{v^2}{8}\right) + \frac{\Gamma(n - v - 2)}{(n - 2)!\Gamma(-v)} \cdot \left(-\frac{v}{4} + \frac{v^2}{8}\right) \right] \\ & \times s(x - n + 1, y) + \frac{\Gamma(n - v - 1)}{(n - 1)!\Gamma(-v)} \cdot \left(-\frac{v}{4} + \frac{v^2}{8}\right) s(x - n, y), \end{aligned} \tag{11}$$

$$\begin{aligned} \frac{\partial^v s(x, y)}{\partial y^v} \cong\ & \left(\frac{v}{4} + \frac{v^2}{8}\right) s(x, y + 1) + \left(1 - \frac{v^2}{2} - \frac{v^3}{8}\right) s(x, y) + \frac{1}{\Gamma(-v)} \\ & \times \sum_{k=1}^{n-2} \left[\frac{\Gamma(k - v - 1)}{(k + 1)!} \cdot \left(\frac{v}{4} + \frac{v^2}{8}\right) + \frac{\Gamma(k - v)}{k!} \cdot \left(1 - \frac{v^2}{4}\right) \right. \end{aligned}$$

$$+\frac{\Gamma(k-v-1)}{(k-1)!}\cdot\left(-\frac{v}{4}+\frac{v^2}{8}\right)\Bigg]s(x,y-k)+\Bigg[\frac{\Gamma(n-v-1)}{(n+1)!\Gamma(-v)}$$
$$\times\left(1-\frac{v^2}{8}\right)+\frac{\Gamma(n-v-2)}{(n-2)!\Gamma(-v)}\left(-\frac{v}{4}+\frac{v^2}{8}\right)\Bigg]s(x,y-n+1)$$
$$+\frac{\Gamma(n-v-1)}{(n-1)!\Gamma(-v)}\cdot\left(-\frac{v}{4}+\frac{v^2}{8}\right)s(x,y-n). \tag{12}$$

For simplicity, we have only used four direction fin the fractional-order gradient operator for the calculation, corresponding to positive $x+$ and $y+$ axis, negative $x-$ and $y-$ axis. Let D^v_{x+}, D^v_{x-}, D^v_{y+}, D^v_{y-} denotes the results for the four directions. The coefficients of the operator in Table 1 and Table 2 are:

$$\begin{cases}
Cs_{-1}=\dfrac{v}{4}+\dfrac{v^2}{8}\\
Cs_0=1-\dfrac{v^2}{2}-\dfrac{v^3}{8}\\
Cs_1=-\dfrac{5v}{4}-\dfrac{5v^3}{16}+\dfrac{v^4}{16}\\
\quad\vdots\\
Cs_k=\dfrac{1}{\Gamma(-v)}\Bigg[\dfrac{\Gamma(k-v-1)}{(k+1)!}\cdot\left(\dfrac{v}{4}+\dfrac{v^2}{8}\right)+\dfrac{\Gamma(k-v)}{k!}\cdot\left(1-\dfrac{v^2}{4}\right)\\
\qquad+\dfrac{\Gamma(k-v-1)}{(k-1)!}\cdot\left(-\dfrac{v}{4}+\dfrac{v^2}{8}\right)\Bigg]\\
\quad\vdots\\
Cs_{n-2}=\dfrac{1}{\Gamma(-v)}\Bigg[\dfrac{\Gamma(n-v-1)}{(n-1)!}\cdot\left(\dfrac{v}{4}+\dfrac{v^2}{8}\right)+\dfrac{\Gamma(n-v-2)}{(n-2)!}\cdot\left(1-\dfrac{v^2}{4}\right)\\
\qquad+\dfrac{\Gamma(n-v-3)}{(n-3)!}\cdot\left(-\dfrac{v}{4}+\dfrac{v^2}{8}\right)\Bigg]\\
\quad\vdots\\
Cs_{n-2}=\dfrac{\Gamma(n-v-1)}{(n+1)!\Gamma(-v)}\cdot\left(1-\dfrac{v^2}{8}\right)+\dfrac{\Gamma(n-v-2)}{(n-2)!\Gamma(-v)}\cdot\left(-\dfrac{v}{4}+\dfrac{v^2}{8}\right)\\
Cs_n=\dfrac{\Gamma(n-v-1)}{(n-1)!\Gamma-v}\cdot\left(-\dfrac{v}{4}+\dfrac{v^2}{8}\right).
\end{cases} \tag{13}$$

4. Numerical Algorithm

Equation (5) contains non-linear penalties for regularization term, so we propose alternating minimization method, based on a half-quadratic splitting (Joshi *et al.*, 2009; Wang *et al.*, 2008; Krishnan and Fergus, 2009; Geman and Yang, 1995; Geman and

Table 1
Operator of x-direction.

$\vdots$	$\vdots$	$\vdots$		$\vdots$		$\vdots$	$\vdots$	$\vdots$
0	0	0	$\cdots$	0	$\vdots$	0	0	0
Cs_{-1}	Cs_0	Cs_1	$\cdots$	Cs_k	$\cdots$	Cs_{n-2}	Cs_{n-1}	Cs_n
0	0	0	$\cdots$	0	$\vdots$	0	0	0
$\vdots$	$\vdots$	$\vdots$		$\vdots$		$\vdots$	$\vdots$	$\vdots$
$\vdots$	$\vdots$	$\vdots$		$\vdots$		$\vdots$	$\vdots$	$\vdots$
0	0	0	$\cdots$	0	$\vdots$	0	0	0
Cs_n	Cs_{n-1}	Cs_{n-2}	$\cdots$	Cs_k	$\cdots$	Cs_1	Cs_0	Cs_{-1}
$\vdots$	$\vdots$	$\vdots$		$\vdots$		$\vdots$	$\vdots$	$\vdots$

Table 2
Operator of y-direction.

$\cdots$	0	Cs_n	0	$\cdots$
$\cdots$	0	Cs_{n-1}	0	$\cdots$
$\cdots$	0	Cs_{n-2}	0	$\cdots$
	$\vdots$	$\vdots$	$\vdots$	
$\cdots$	0	Cs_n	0	$\cdots$
	$\vdots$	$\vdots$	$\vdots$	
$\cdots$	0	Cs_1	0	$\cdots$
$\cdots$	0	Cs_0	0	$\cdots$
$\cdots$	0	Cs_{-1}	0	$\cdots$
$\cdots$	0	Cs_{-1}	0	$\cdots$
$\cdots$	0	Cs_0	0	$\cdots$
$\cdots$	0	Cs_1	0	$\cdots$
	$\vdots$	$\vdots$	$\vdots$	
$\cdots$	0	Cs_k	0	$\cdots$
	$\vdots$	$\vdots$	$\vdots$	
$\cdots$	0	Cs_{n-2}	0	$\cdots$
$\cdots$	0	Cs_{n-1}	0	$\cdots$
$\cdots$	0	Cs_n	0	$\cdots$

Reynolds, 1992) to solve it. Estimation variable e between $\mathbf{X} \otimes \mathbf{h}$ and $\mathbf{Y}$ and auxiliary variable $\mathrm{w} = (w_x, w_y)$ are introduced, so the objective function in Eq. (5) can be modified as

$$(\hat{\mathbf{X}}, \hat{e}, \hat{\mathbf{w}}) = \arg\min_{\mathbf{X},e,\mathbf{w}} \sum_i \left(\frac{1}{2\eta} \|\mathbf{x}_i \otimes \mathbf{h} - \mathbf{y}_i - e\|^2 + \frac{1}{2\theta} \left(\left\| \nabla_x^v \mathbf{x}_i - w_{x,i} \right\|_2^2 + \left\| \nabla_y^v \mathbf{x}_i - w_{y,i} \right\|_2^2 \right) + \lambda \left(|w_{x,i}|^\beta + |w_{y,i}|^\beta \right) + \|e\| \right), \tag{14}$$

where F the auxiliary variable $\mathbf{w}$ at each pixel that allow us to move the $\nabla_x^v \mathbf{x}_i$ and $\nabla_y^v \mathbf{x}_i$ outside the $|.|^\beta$ expression, η and θ are the weight parameters. When $\theta \to 0$, the solution of Eq. (14) converges to that of Eq. (5). To solve Eq. (14), Alternating Minimization method is introduced, where solve $\mathbf{X}$ e $\mathbf{w}$ independently, fixed $\mathbf{e}$ $\mathbf{w}$ to solve $\mathbf{X}$. The initial value $\mathbf{e}$ and $\mathbf{w}$ both are zeros, the initial value of $\mathbf{X}$ is the observed image intensity.

There are two step to compute unknown variables in each iteration. In first step, compute $\mathbf{X}$ given estimated value $\mathbf{e}$ and $\mathbf{w}$ from previous iteration by minimizing

$$\hat{\mathbf{X}} = \arg\min_{\mathbf{X}} \|\mathbf{X} \otimes \mathbf{h} - \mathbf{Y} - \mathbf{E}\|^2 + \frac{\eta}{\theta} \left\| \nabla^v \mathbf{X} - \mathbf{w} \right\|_2^2. \tag{15}$$

Equation (15) is a quadratic and according to *Parseval*'s theorem, the optimal $\mathbf{X}$ can be computed from Eq. (16)

$$X = F^{-1}\left(\frac{\overline{F(\mathbf{h})} F(\mathbf{Y} + e) + \eta/\theta (\overline{F(\partial_x^v)} F(w_x) + \overline{F(\partial_y^v)} F(w_y))}{\overline{F(\mathbf{h})} F(\mathbf{h}) + \eta/\theta (\overline{F \partial_x^v}) F(\partial_x^v) + \overline{F(\partial_y^v)} F(\partial_y^v)} \right), \tag{16}$$

where $F(.)$ and $F^{-1}(.)$ denote the Fourier transform and inverse Fourier transform, respectively and $\overline{F(.)}$ is the complex conjugate operator.

Secondly, compute $\mathbf{E}$'s and $\mathbf{w}$'s optimization, based on the value of $\mathbf{X}$ estimated in first step. However, they are independent variables so that their optimization are independent too. For e, objective function is minimized

$$\hat{e} = \arg\min_{e} \frac{1}{2} \left\| e - (\mathbf{X} \otimes \mathbf{h} - \mathbf{Y}) \right\|^2 + \eta \|e\|. \tag{17}$$

Then the value e is gotten as

$$e = \text{sign}(\mathbf{X} \otimes \mathbf{h} - \mathbf{Y}) \max\left(\left\| e - (\mathbf{X} \otimes \mathbf{h} - \mathbf{Y}) \right\| - \eta, 0 \right). \tag{18}$$

The value $\mathbf{w}$ can be computed by minimizing objective function in Eq. (19)

$$\hat{\mathbf{w}} = \arg\min_{\mathbf{w}} \frac{1}{2} \left\| \mathbf{w} - \partial^v \mathbf{X} \right\|_2^2 + \theta \lambda \|w\|^\beta. \tag{19}$$

For $\beta = 2$, the solution of $\mathbf{w}$ is quadratic problem and $\beta = 1$, the value of $\mathbf{w}$ can be derived according to the shrinkage formula. And in Wright *et al.* (2009) the special cases of $1 < \beta < 2$ are analyzed and (Krishnan and Fergus, 2009) address the case $0 < \beta < 1$. Their excellent algorithms and open source code are applied in our algorithm. Empirically set $\eta_0 = 1$, $\theta_0 = \lambda^{-1}$ and $\eta_{threshold} = \theta_{threshold} = 1e - 2$. Figure 4(a) shows tested blurry photos. Figure 4(b) proves that our algorithm can restore latent image successfully. More experiments compared to other state-of-the-art image deconvolution will be showed in next section.

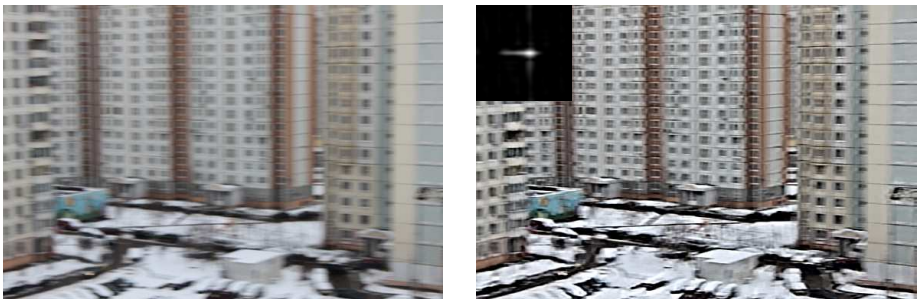

(a) (b)

Fig. 4. Image deconvolution: (a) blurred image; (b) restore image using our algorithm.

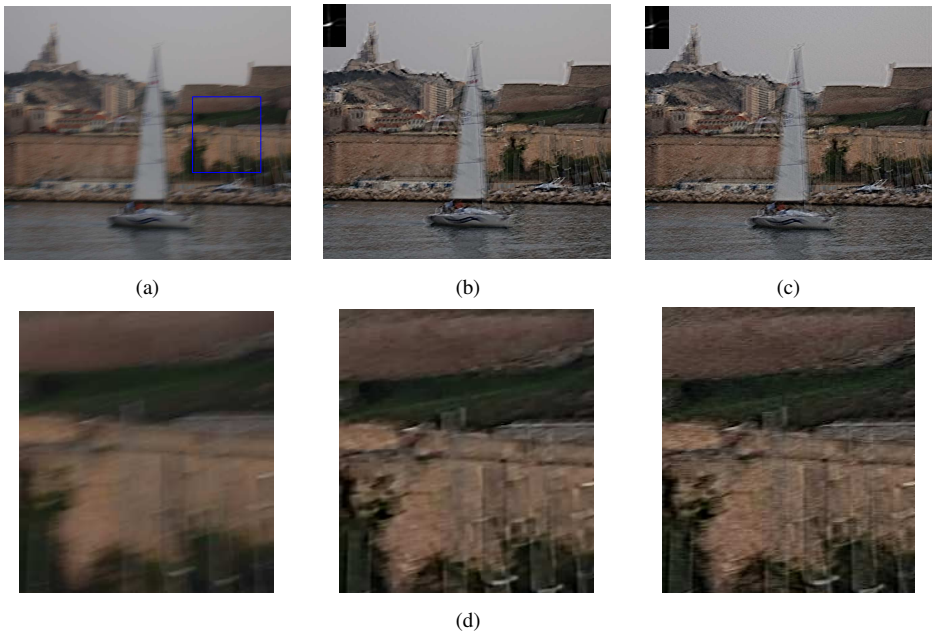

(a) (b) (c)

(d)

Fig. 5. Testing our algorithm with real-life motion blurry images: (a) blurry image; (b) restored image by using the algorithm in Krishnan *et al.* (2011); (c) restored image by our algorithm; (d) details comparison on image window, left: details in (a), middle: details in (b) and right: details in (c).

5. More Experiments

In this section the proposed blind deconvolution algorithms is tested with real-life blurry image. The tested images are provided in the online image database in Xu and Jia (2010). As before, we use algorithm to estimate kernel.

We compare the result with the method described in Krishnan *et al.* (2011). In Figs. 5(a) and 6(a) shows the burry image caused by camera shake. Figures 5(b) and 6(b) show that Krishnan *et al.* (2011) reconstruct latent image with sharp edge and smooth

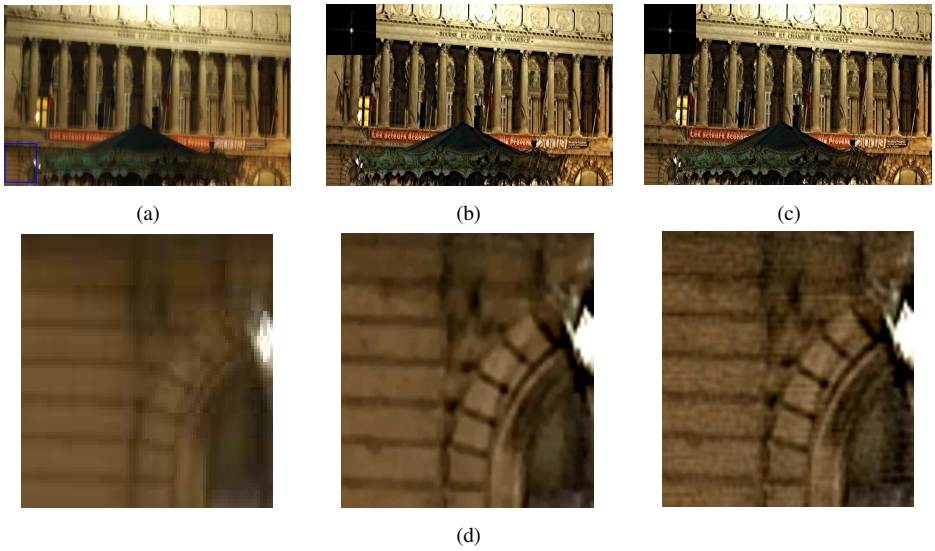

Fig. 6. Testing our algorithm with real-life motion blurry images: (a) blurry image; (b) restored image by using the algorithm in Krishnan *et al.* (2011); (c) restored image by our algorithm; (d) details comparison on image window, left: details in (a), middle: details in (b) and right: details in (c).

region and without textural details in smooth region. Our result in Figs. 5(c) and 6(c) not only preserves sharp edge and smooth regions, but keep the textural features in the smooth area, so that the visual quality is improved. There are comparison in details in Figs. 5(d) and 6(d) the textural features in the smooth image.

In our experiments, the fractional-order $v = 0.3$ in Fig. 5, $v = 0.4$ in Fig. 6.

6. Conclusion

In this paper, we discuss the reason why algorithms using natural image gradient fail to reconstruct image textural details by analyzing 1D signal restoration and exploit the fractional-order gradient to deal with image texture. We show that the fractional-order gradient image prior can restore piece-wise smooth regions without over-smoothing textured regions, improving the visual quality of reconstructed images as verified by our experiments. However, in fact, different textures have different fractional-order gradient statistics even with an image, so our further work is to extend the current research by adapting to textural characteristics.

Acknowledgments. This work is supported by National Basic Research Program of China (973 Program) (No. 2014CB360506), Sichuan Province Science and Technology Support Program (No. 2015RZ0008), Educational Commission of Sichuan Province of China (No. 15ZA0186) and National Natural Science Foundation of China (NSFC) (No. 61302028).

References

Bai, J., Feng, X.-C. (2007). Fractional-order anisotropic diffusion for image denoising. *IEEE Transactions on Image Processing*, 16(10), 2492–2502.

Bar, L., Sochen, N., Kiryati, N. (2005). Image deblurring in the presence of salt-and-pepper noise. *Scale Space and PDE Methods in Computer Vision*, 107–118.

Calvo-Rolle, J.L., Fontenla-Romero, O., PÍęz-SÍnchez, B. (2014). Adaptive inverse control using an online learning algorithm for neural networks. *Informatica*, 25(3), 401–414.

Chan T.F., Wong, C.K. (1998). Total variation blind deconvolution. *IEEE Transactions on Image Processing*, 7(3), 370–375.

Chan, R.H., Lanza, A., Morigi, S., Sgallari, F. (2013). An adaptive strategy for the restoration of textured images using fractional order regularization. *Numerical Mathematics: Theory, Methods and Applications*, 6(1), 276–296.

Fergus, R., Singh, B., Hertzmann, A., Roweis, S.T., Freeman, W.T. (2006). Removing camera shake from a single photograph. *ACM Transactions on Graphics (TOG)*, 25, 787–794.

Geman, D., Reynolds, G. (1992). Constrained restoration and the recovery of discontinuities. *IEEE Transactions on Pattern Analysis and Machine Intelligence*, 14(3), 367–383.

Geman, D., Yang, C. (1995). Nonlinear image recovery with half-quadratic regularization. *IEEE Transactions on Image Processing*, 4(7), 932–946.

Haykin, S.S. (1994). *Blind deconvolution*. PTR Prentice Hall, New York.

Joshi, N., Zitnick, C.L., Szeliski, R., Kriegman,D.J. (2009). Image deblurring and denoising using color priors. In: *IEEE Conference on Computer Vision and Pattern Recognition (CVPR 2009)*, IEEE Pres, New York, pp. 1550–1557.

Jun, Z., Zhihui, W. (2011). A class of fractional-order multi-scale variational models and alternating projection algorithm for image denoising. *Applied Mathematical Modelling*, 35(5), 2516–2528.

Krishnan, D., Fergus, R. (2009). Fast image deconvolution using hyper-Laplacian priors. *Advances in Neural Information Processing Systems*, 22, 1–9.

Krishnan, D., Tay, T., Fergus, R. (2011). Blind deconvolution using a normalized sparsity measure. In: *IEEE Conference on Computer Vision and Pattern Recognition (CVPR 2011)*, IEEE Press, New York, pp. 233–240.

Levin, A., Weiss, Y., Durand, F., Freeman, W.T. (2009). Understanding and evaluating blind deconvolution algorithms. In: *IEEE Conference on Computer Vision and Pattern Recognition. (CVPR 2009)*, IEEE Press, New York, pp. 1964–1971.

Pu, Y., Wang, W., Zhou, J., Wang, Y., Jia, H. (2008). Fractional differential approach to detecting textural features of digital image and its fractional differential filter implementation. *Science in China Series F: Information Sciences*, 51(9), 1319–1339.

Rao, Y., Chen, L. (2012). A survey of video enhancement techniques. *Journal of Information Hiding and Multimedia Signal Processing*, 3(1), 71–99.

Rudin, L.I., Osher, S. (1994). Total variation based image restoration with free local constraints. In: *Proceedings of the IEEE International Conference on Image Processing, 1994 (ICIP-94.)*, Vol. 1. IEEE, pp. 31–35.

Sekko, E., Thomas, G., Boukrouche, A. (1999). A deconvolution technique using optimal wiener filtering and regularization. *Signal Processing*, 72(1), 23–32.

Wang, Y., Yang, J., Yin, W., Zhang, Y. (2008) A new alternating minimization algorithm for total variation image reconstruction. *SIAM Journal on Imaging Sciences*, 1(3), 248–272 .

Wright, S.J., Nowak, R.D., Figueiredo, M.A. (2009). Sparse reconstruction by separable approximation. *IEEE Transactions on Signal Processing*, 57(7), 2479–2493.

Xu, L., Jia, J. (2010). Two-phase kernel estimation for robust motion deblurring. In: *Computer Vision—ECCV 2010*, pp. 157–170.

Yi-Fei, P. (2007). Fractional differential analysis for texture of digital image. *Journal of Algorithms & Computational Technology*, 1(3), 357–380.

Zhang, Y., Pu, Y.-F., Hu, J.-R., Liu, Y., Zhou, J.-L. (2011). A new ct metal artifacts reduction algorithm based on fractional-order sinogram inpainting. *Journal of X-ray science and technology*, 19(3), 373–384.

Zhang, Y., Pu, Y., Hu, J., Zhou, J. (2012). A class of fractional-order variational image inpainting models. *Applied Mathematics*, 6(2), 299–306.

Y. Fu is a Lecturer at School of Computer Science, Chengdu University of Information Technology of China. She has been duly granted degree of master and PhD from School of Computer Science, Sichuan University. Her research interest covers image processing and pattern recognization.

X. Wu is a Vice Professor at School of Computer Science, Chengdu University of Information Technology of China. His research interest covers medical image processing.

X. Li is a Vice Professor at School of Computer Science, Sichuan University of China. Her research interest covers image processing and face recognization.

K. He is a Vice Professor at School of Computer Science, Sichuan University of China. His research interest covers image processing and face recognization.

Y. Zhang is a Vice Professor at School of Computer Science, Sichuan University of China. His research interest covers medical image processing.

J. Zhou is a Professor at His research interest covers image processing pattern recognization and intellectual computing.

Judesio vaizdo atkūrimas taikant originalaus vaizdo trumpeninės eilės gradientą

Ying FU, Xi WU, Xiaohua LI, Kun HE, Yi ZHANG, Jiliu ZHOU

Pradinės informacijos apie originalų vaizdą pasirinkimas, lemia atkurto vaizdo kokybę. Naujausi vaizdų apdorojimo algoritmai latentinio vaizdo su daliniais tolydžiais regionais atkūrimui, kaip pradinę informaciją apie vaizdo originalą, naudoja gradientų paskirstymo funkciją su „sunkia uodega“ (angl. heavy-tailed). Tačiau, tokia pirminė informacija panaikina vaizde vidutinio dažnio komponentes, tokias kaip tekstūros detales, nors išsaugo aštrius jos kraštus.

Siekiant atkurti tekstūros detales latentiniame vaizde kaip pradinę informaciją apie vaizdo originalą siūloma taikyti trumpeninės eilės gradientą, kuris yra labiau tinkamas vaizdo tekstūroms charakteristikoms aprašyti. Eksperimentiniai tyrimai parodė, kad atkurtame vaizde tekstūrų detalės matomos aiškiau, pagerėja vizualinė kokybė.